Band structures in ^{108}Ag

F. R. Espinoza-Quiñones, E. W. Cybulska, L. G. R. Emediato, C. L. Lima,
N. H. Medina,* J. R. B. Oliveira, M. N. Rao, R. V. Ribas, M. A. Rizzutto, W. A. Seale, and C. Tenreiro†
Laboratório Pelletron, Depto. de Física Nuclear, Instituto de Física, Universidade de São Paulo, Caixa Postal 20516, 01452-990, São Paulo, Brazil
(Received 24 February 1995)

The ^{108}Ag nucleus has been studied by in-beam γ spectroscopy with the heavy-ion fusion-evaporation reaction ^{100}Mo(^{11}B,3$n\gamma$) at 39 MeV. Excitation functions, γ-γ-t coincidences, angular distributions, and DCOQ ratios were measured. A level scheme has been constructed and various bands have been identified with characteristics similar to those in other $A \approx 100$ nuclei. Total Routhian surface calculations predict prolate axially symmetric shapes with collective and noncollective character and satisfactorily account for most of the experimental results.

PACS number(s): 21.10.Re, 23.20.Lv, 27.60.+j

I. INTRODUCTION

In recent years, the influence of the high-j intruder orbits on the deformation of γ-soft nuclei has been studied in various mass regions such as $A \approx 100$, 130, 150, and 190. In each of these regions the Fermi levels for the protons and the neutrons are in different parts of an intruder subshell. In odd-odd nuclei, this leads in general to conflicting tendencies of the proton and neutron intruder quasiparticles, one of these being coupled mainly to the rotational axis and the other to the deformation axis. Several interesting phenomena have emerged in this context, such as triaxiality, shape transitions, shape coexistence, oblate bands, etc. The phenomenon of signature inversion, first observed in $A \approx 150$ odd nuclei at high spin, is also seen in odd-odd nuclei at relatively low spins and, despite several attempts, has not been fully understood [1]. In the $A \approx 100$ odd-odd nuclei, the active intruder orbits are near the top of the $\pi g_{9/2}$ and the bottom of the $\nu h_{11/2}$ subshells. The former orbits are oblate driving, while the latter are strongly prolate driving and favor increased elongations.

In this paper we present an investigation of ^{108}Ag by a heavy-ion induced reaction. Various bands were identified which resemble previously observed structures in neighboring odd-odd Ag isotopes. In particular, the $\pi g_{9/2} \otimes \nu h_{11/2}$ band, which has been systematically seen in the ^{102,104,106}Ag [2–4] and the corresponding Rh isotones [5] and also in the present work in ^{108}Ag. In both ^{106}Ag and ^{108}Ag the ($I^\pi = 1^+$) ground state and the ($I^\pi = 6^+$) isomeric states have been assigned $\pi g_{9/2} \otimes \nu d_{5/2}$ configuration. Similar bandlike structures (based on this 6^+ state) were observed in both nuclei. Another band resembles the $\pi(p_{1/2}, f_{5/2})$ bands seen in odd-A Ag isotopes [6,7] and thus has been tentatively assigned the $\pi(p_{1/2}, f_{5/2}) \otimes \nu h_{11/2}$ configuration. Total Routhian surface (TRS) calculations of the Strutinsky type with a cranked Woods-Saxon potential with pairing were performed and indicate a stabilization of the quadrupole deformation around $\beta_2 = 0.16$, $\gamma = 0°$ (prolate collective) for all configurations containing at least one $h_{11/2}$ quasineutron excitation. For the $\pi g_{9/2} \otimes \nu d_{5/2}$ configuration an equilibrium deformation around $\beta_2 = 0.1$, $\gamma = -120°$ (prolate, noncollective) is predicted and can probably be associated with the 6^+ isomer bandhead. In addition a structure was observed with characteristics of high-K bands (probably $K = 8$).

II. EXPERIMENTAL PROCEDURE

High-spin states in ^{108}Ag were populated by the ^{100}Mo(^{11}B,3$n\gamma$) reaction. The beam was provided by the Pelletron Accelerator of the University of São Paulo. The target used was a ~ 20 mg/cm^2 metallic self-supporting foil of enriched ^{100}Mo.

The γ-ray measurements included excitation functions, angular distributions, and γ-γ coincidences and were obtained with HPGe detectors having $\sim 20\%$ efficiencies and energy resolutions of 2.1–2.4 keV at 1332 keV. The excitation functions were obtained by varying the beam energy in steps of 5 MeV from 35 to 50 MeV. The peak cross section of the desired (^{11}B,3n) reaction is near the Coulomb barrier (34 MeV) and substantial contribution from the 4n channel was observed, which is in reasonable agreement with the statistical model calculations (PACE). A beam energy of 39 MeV was chosen for the other measurements. This energy was the best compromise between the enhancement of population of high-spin states and the competition from the 4n channel. The 4n channel (^{107}Ag) has a well-established decay scheme [6,4], permitting the identification of its γ rays. Other very weak channels such as 2$n\alpha$ and 4np were also observed.

*Present address: Istituto Nazionale di Fisica Nucleare, Sezione di Padova, Padova, Italy.
†Present address: Facultad de Ciencias, Depto. de Física, Universidad de Chile, Santiago de Chile, Chile.

The coincidence data were obtained with two BGO Compton suppressed HPGe detectors placed at ±50° and two HPGe detectors at ±140° to the beam direction. At least one of a set of one 4 in. × 4 in. NaI(Tl) and seven 3 in. × 3 in. detectors placed, respectively, above and below the target, was required to trigger for an accepted γ-γ coincidence event. The angular distribution data were taken using a Compton suppressed HPGe detector positioned at four angles varying from 0° to +90° and a second HPGe detector at −90° was used as a monitor. Due to the complexity of the singles spectra, it was possible to obtain reliable angular distributions only for the strong M1 transitions of the yrast band.

The total number of γ-γ coincidence events was about 7×10^7 and the data were gain matched and sorted into two-dimensional arrays. A symmetrized $E_\gamma \times E_\gamma$ matrix was constructed and the analysis of the data was performed using PANORAMIX [8] and VAXPAK [9] codes.

TABLE I. Energies, spin assignments, relative intensities, and DCOQ ratios for the γ-ray transitions in the ^{100}Mo(^{11}B,3n)^{108}Ag reaction at 39 MeV. The γ-ray energies are accurate to ± 0.3 keV. E_i and E_f are the energies of the initial and final states corresponding to each transition.

E_γ [keV]	E_i [keV]	E_f [keV]	$I_i^\pi \rightarrow I_f^\pi$	I_γ	DCOQ ratio	E_γ [keV]	E_i [keV]	E_f [keV]	$I_i^\pi \rightarrow I_f^\pi$	I_γ	DCOQ ratio
35.3	533.8	498.5	$(8^-) \rightarrow (7^-)$	10.0(20)		506.7	1942.4	1435.7	$(12^-) \rightarrow (11^-)$	41.8 (9)	0.53 (8)
54.8	420.7	366.3		4.0(10)		532.6	4092.1	3559.5	$(16^-) \rightarrow (15^-)$	6.4 (9)	
58.5	498.5	440.1	$(7^-) \rightarrow (6^-)$	23.6(9)		537.4	2908.9	2371.1	$(13^+) \rightarrow (11^+)$	5.3 (9)	
75.5	366.3	290.8				550.9	2994.9	2444.0	$(14^-) \rightarrow (13^-)$	10.3 (9)	0.65 (9)
75.5	290.8	215.0				557.0	1091.0	533.8	$(10^-) \rightarrow (8^-)$	5.3 (8)	
75.0	810.1	735.3	$(8^+) \rightarrow (7^+)$	9.0(20)		570.8	1490.2	919.4	$(9^+) \rightarrow (8^+)$	7.2 (9)	
103.1	523.8	420.7		10.4 (5)	0.96 (10)	564.6	3559.5	2994.9	$(15^-) \rightarrow (14^-)$	7.0 (9)	0.59 (14)
117.8	919.4	802.0	$(8^+) \rightarrow (7^+)$	5.6 (4)	0.62 (14)	573.6	4179.7	3606.1	$(16^-) \rightarrow (15^-)$	4.7 (9)	
122.6	498.5	376.2	$(7^-) \rightarrow (7^+)$	1.7 (4)		585.4	3494.7	2908.9	$(15^+) \rightarrow (13^+)$	3.6 (9)	
148.2	523.9	376.1	$(6^+) \rightarrow (7^+)$	4.1 (5)	0.42 (12)	595.1	2536.9	1942.4	$(12^-) \rightarrow (12^-)$	6.0 (9)	
153.9	687.7	533.8	$(9^-) \rightarrow (8^-)$	81.5 (9)	0.64 (9)	623.7	734.6	110.9	$(7^+) \rightarrow (6^+)$	5.7 (9)	
157.6	533.8	376.2	$(8^-) \rightarrow (7^+)$	4.2 (7)		688.2	1490.2	802.0	$(9^+) \rightarrow (7^+)$	6.3 (9)	
157.9	523.8	366.3		1.9 (4)	0.69 (14)	692.0	2064.1	1372.3	$(10^+) \rightarrow (9^+)$	5.4 (9)	
183.5	1674.2	1490.2	$(10^+) \rightarrow (9^+)$	1.5 (4)		697.0	2371.1	1674.2	$(11^+) \rightarrow (10^+)$	3.2 (9)	
215.5	215.0	0.0	$3^+ \rightarrow 1^+$	7.3 (5)	1.00 (18)	699.2	810.1	110.9	$(8^+) \rightarrow 6^+$	5.3 (9)	
233.3	2908.9	2675.5	$(13^+) \rightarrow (12^+)$	13.1 (6)	0.71 (6)	700.1	3872.7	3172.3	$(16^+) \rightarrow (14^+)$	4.0 (9)	
234.0	2536.9	2302.9	$(12^-) \rightarrow (11^-)$	4.8 (6)		722.0	1098.2	376.2	$(8^+) \rightarrow (7^+)$	12.2 (13)	
240.4	2908.9	2668.6	$(13^+) \rightarrow (12^+)$	7.3 (5)	0.70 (10)	748.0	1435.6	687.4	$(11^-) \rightarrow (9^-)$	15.4 (11)	0.90 (12)
249.2	2675.5	2426.8	$(12^+) \rightarrow (11^+)$	4.0 (6)	0.59 (17)	754.8	1674.2	919.4	$(10^+) \rightarrow (8^+)$	37.7 (12)	1.08 (18)
255.4	366.3	110.9		10.7 (5)	0.61 (8)	818.0	4313.2	3494.7	$(17^+) \rightarrow (15^+)$	3.4 (8)	
261.8	2536.9	2275.1	$(12^-) \rightarrow (11^-)$	3.0 (5)		851.2	1942.3	1090.8	$(12^-) \rightarrow (10^-)$	9.5 (11)	0.82 (17)
263.4	3172.3	2908.9	$(14^+) \rightarrow (13^+)$	17.7 (6)	0.69 (6)	880.9	2371.1	1490.2	$(11^+) \rightarrow (9^+)$	5.0 (9)	
265.3	376.2	110.9	$(7^+) \rightarrow 6^+$	19.9 (7)	0.63 (11)	895.3	2536.9	1641.7	$(12^-) \rightarrow (10^-)$	5.2 (9)	
278.2	802.0	523.8	$(7^+) \rightarrow (6^+)$	4.9 (5)	0.46 (16)	934.6	1669.9	735.3	$(9^+) \rightarrow (7^+)$	4.4 (11)	
304.5	2675.5	2371.1	$(12^+) \rightarrow (11^+)$	4.2 (6)		936.6	2426.8	1490.2	$(11^+) \rightarrow (9^+)$	4.2 (9)	
310.7	2847.6	2536.9	$(13^-) \rightarrow (12^-)$	6.3 (6)	0.57 (15)	954.0	1641.5	687.4	$(10^-) \rightarrow (9^-)$	9.5 (9)	0.73 (13)
322.4	3494.7	3172.3	$(15^+) \rightarrow (14^+)$	14.5 (7)	0.75 (9)	965.9	2064.1	1098.2	$(10^+) \rightarrow (8^+)$	4.6 (9)	
329.2	440.1	110.9	$(6^-) \rightarrow 6^+$	100.0 (9)	0.84 (9)	977.2	1787.3	810.1	$(10^-) \rightarrow (8^-)$	6.7 (9)	
340.8	3188.4	2847.6	$(14^-) \rightarrow (13^-)$	6.2 (6)	0.83 (18)	987.0	1098.2	110.9	$(8^+) \rightarrow 6^+$	5.6 (12)	
344.7	1435.7	1091.0	$(11^-) \rightarrow (10^-)$	48.4 (9)	0.59 (9)	992.0	4179.7	3188.4	$(16^-) \rightarrow (14^-)$	1.7 (7)	
359.1	735.3	376.2	$(7^+) \rightarrow (7^+)$	5.9 (7)		994.4	2668.6	1674.2	$(12^+) \rightarrow (10^+)$	15.5 (12)	1.00 (19)
361.0	2302.9	1942.4	$(11^-) \rightarrow (12^-)$	2.2 (6)		996.1	1372.3	376.2	$(9^+) \rightarrow (7^+)$	5.7 (12)	
378.0	3872.7	3494.7	$(16^+) \rightarrow (15^+)$	10.9 (5)	0.86 (20)	999.3	2371.6	1372.3	$(11^+) \rightarrow (9^+)$	5.4 (10)	
387.5	498.5	110.9	$(7^-) \rightarrow (6^+)$	10.5 (7)	0.67 (10)	1001.3	2675.5	1674.2	$(12^+) \rightarrow (10^+)$	18.6 (11)	0.89 (16)
393.2	2536.9	2143.7	$(12^-) \rightarrow (11^-)$	8.3 (7)	0.62 (14)	1008.5	2444.1	1435.6	$(13^-) \rightarrow (11^-)$	11.0 (10)	0.93 (14)
395.6	919.4	523.8	$(8^+) \rightarrow (6^+)$	32.3 (9)	0.91 (14)	1041.0	2710.9	1669.9	$(11^+) \rightarrow (9^+)$	5.3 (12)	
403.3	1091.0	687.7	$(10^-) \rightarrow (9^-)$	72.7 (9)	0.70 (9)	1052.5	2995.0	1942.3	$(14^-) \rightarrow (12^-)$	7.0 (11)	
412.9	523.8	110.9	$(6^+) \rightarrow 6^+$	16.4 (8)	0.90 (12)	1052.8	2143.3	1090.8	$(11^-) \rightarrow (10^-)$	2.5 (5)	
417.7	3606.1	3188.4	$(15^-) \rightarrow (14^-)$	5.8 (6)		1096.8	4092.0	2995.0	$(16^-) \rightarrow (14^-)$	3.0 (9)	
425.8	802.0	376.2	$(7^+) \rightarrow (7^+)$	7.2 (7)	0.93 (27)	1101.8	2536.6	1435.6	$(12^-) \rightarrow (11^-)$	3.8 (9)	
434.3	810.1	376.2	$(8^+) \rightarrow (7^+)$	13.0 (9)		1108.0	1641.5	533.5	$(10^-) \rightarrow (8^-)$	3.0 (9)	
440.5	4313.2	3872.7	$(17^+) \rightarrow (16^+)$	5.5 (7)	0.68 (17)	1115.2	3559.5	2444.1	$(15^-) \rightarrow (13^-)$	4.7 (9)	
496.5	3172.3	2675.5	$(14^+) \rightarrow (12^+)$	5.6 (9)		1117.3	2904.6	1787.3	$(12^+) \rightarrow (10^+)$	4.3 (8)	
501.6	2444.0	1942.4	$(13^-) \rightarrow (12^-)$	15 (3)	0.62 (9)	1184.0	2275.1	1091.0	$(11^-) \rightarrow (10^-)$	4.8 (8)	
502.0	2143.7	1641.7	$(11^-) \rightarrow (10^-)$	6 (1)	0.58 (21)						

Background subtracted gate spectra were generated, and efficiency corrected relative intensities of the γ rays were extracted. Typical examples of coincidence spectra are shown in Fig. 1. The energy and efficiency calibration for the spectra were made using ^{152}Eu and ^{133}Ba lines. The intensities of γ rays in Table I were extracted from the γ-γ coincidence data and represent the sum of the efficiency corrected areas of the transitions (placed in the level scheme) in coincidence with each gate of energy E_γ.

The multipolarities for most of the γ rays were obtained applying the DCOQ method (directional correlation from oriented states referred to quadrupole transitions) [10]. An $E_\gamma(\pm 50°) \times E_\gamma(\pm 140°)$ matrix was constructed to extract multipolarity information from the two coincidence intensities $N_{12}(\gamma_1 \rightarrow \pm 50°, \gamma_2 \rightarrow \pm 140°)$ and $N_{21}(\gamma_2 \rightarrow \pm 50°, \gamma_1 \rightarrow \pm 140°)$. The DCOQ$(\gamma_1, \gamma_2)$ ratios (N_{21}/N_{12}) corrected for relative efficiencies of detectors at $\pm 140°$ and $\pm 50°$ are referred to quadrupole transition gate (γ_2) and reflect the multipolarity and mixing ratio of γ_1. The sum of gates on several quadrupole transitions was used in order to determine the DCOQ ratios of weak γ-ray transitions. The theoretical DCOQ ratio depends on the pair of fixed observation angles, multipole character of the transition γ_1, the ΔI involved, and on the orientation of the spin of the initial state of the cascade. For cascades of predominantly stretched transitions there is very little dependence on the particular state depopulated by transition γ_1 [11]. Therefore the DCOQ ratios for transitions with pure multipolarities (L) can be estimated from the values of L and ΔI. Table II shows the ratios calculated specifically for the present measurements. It should be pointed out that $\Delta I = 1$ transitions could give DCOQ ratios less than or greater than 0.85 for $\delta < 0$ or $\delta > 0$, respectively. Also, $\Delta I = 0$ transitions could give a DCOQ ratio between 0.81 and 1.03 for large mixing ratios.

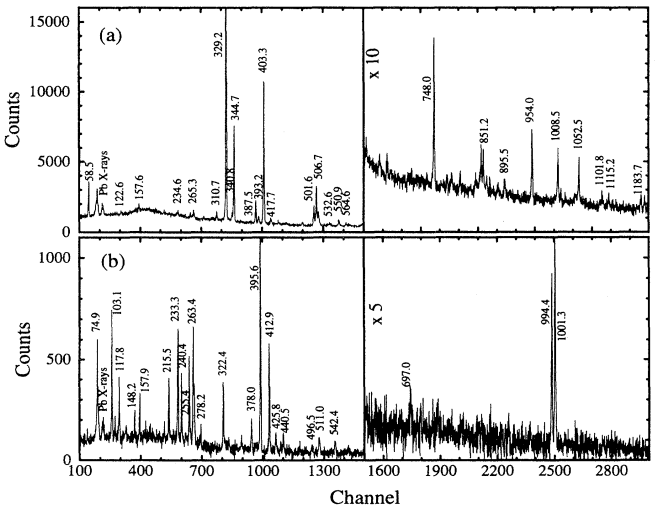

FIG. 1. Background-subtracted γ-γ coincidence spectra of the ^{100}Mo(^{11}B,3n)^{108}Ag reaction at 39 MeV gated by (a) the 153.9 keV line and (b) the 754.8 keV line.

TABLE II. Theoretical DCOQ ratios for mixing ratio δ=0. L is the multipolarity of the γ ray involved and ΔI is the spin change in the transition.

L	ΔI	DCOQ ratio
1	0	1.03
1	1	0.85
2	0	0.81
2	1	0.98
2	2	1.00

III. EXPERIMENTAL RESULTS

A. Level scheme

The level scheme of ^{108}Ag, shown in Fig. 2, was constructed on the basis of the γ-γ coincidence relations and intensity-energy balances. The relative intensities of the γ rays belonging to ^{108}Ag and the measured DCOQ ratios are listed in Table I, together with the level energies and their proposed spins and parities. Six structures with rotational band characteristics can be observed in the level scheme. Negative parity bands with strong $M1$ and weak $E2$ transitions and a small staggering (e.g., band 1) are typical of this mass region. On the other hand, bands 3, 4, and 5, show strong $E2$ with very weak $M1$'s transitions and a large staggering (200–400 keV).

In ^{108}Ag, the spin and parity of the $I^\pi = 1^+$ ground

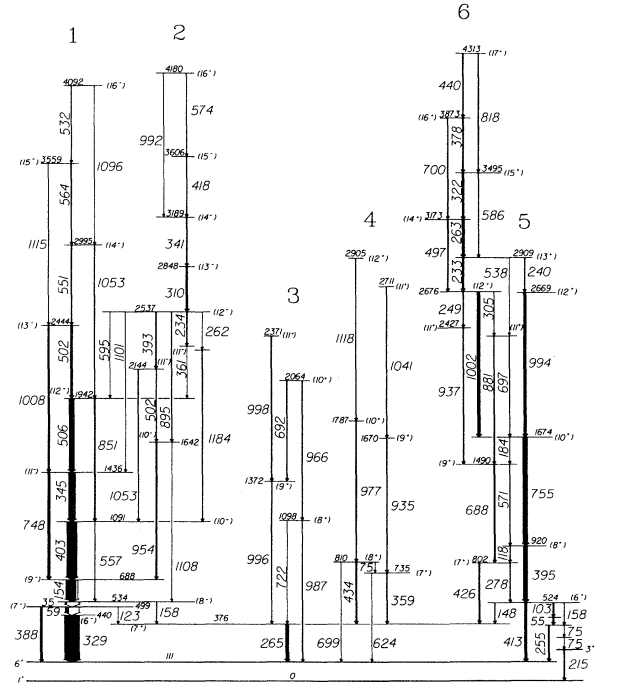

FIG. 2. The level scheme of ^{108}Ag obtained from the ^{100}Mo(^{11}B,3$n\gamma$) reaction at 39 MeV.

TABLE III. The assigned K values and configurations in ^{108}Ag. The signature splittings listed were taken at $\hbar\omega$=0.35 MeV.

Band	K	(π, α)	Configuration	$\Delta e'_{\rm exp}$ (keV)
1	4	(-,0); (-,-1)	$aA; bA$	60
2	4	(-,0); (-, 1)	$aAEF; bAEF$	0
3	0	(+,0); (+, 1)	$aG; aH(aG; bG)$	250
4	0	(+,0); (+, 1)	$aE; aF(aE; bE)$	350
5	0	(+,0); (+, 1)	$gA; hA$	180
6	8	(+,0); (+, 1)	$gacA$	0

state and of the two isomeric states at 110.9 keV ($I^\pi = 6^+$) and at 215 keV ($I^\pi = 3^+$) are well known from atomic beam resonance [12], from the β decay properties to Pd and Cd isotopes [13] and from $(p, n\gamma)$ reactions [14]. The assignments of the other spins in the level scheme were made on the basis of the DCOQ ratios and the systematics for this mass region. The 533.8-keV level of the negative parity band 1 decays through two low energy γ rays of 35 and 59 keV. A similar decay has been also observed in other Ag and Rh isotopes [2,3,5]. Taking into account electron conversion coefficients, the intensity balance shows that the 35- and 59-keV transitions are necessarily of $M1$ nature. The DCOQ ratio indicates a dipole of $\Delta I = 1$ type for the 388-keV transition. Since this transition populates the 6^+ isomer at 110.9 keV we propose $I^\pi = 7^-$ for the 498.5 keV level, and $I^\pi = 6^-$ for the 440.1 keV level. This choice of spins is also consistent with the similar level scheme of ^{106}Ag [2]. The remaining attributions of the spins in band 1 were based on angular distributions, DCOQ ratios, and rotational band characteristics.

In the case of band 2, according to the DCOQ ratios, the transitions of 954, 502, and 393 keV are of type $\Delta I = 0$ or 1. Therefore the maximum spin of the 2536.9 keV level is $I = 12$. The value of $I = 12$ was chosen in order to maintain band 2 nearest to the yrast line. The DCOQ ratio for the 265-keV γ ray which feeds the 6^+ isomer (the bandhead of band 3) indicates a change of no more than one unit of spin. Besides this, the proposed spins for the levels of band 3 were chosen in analogy to a similar structure in ^{106}Ag. The bandhead of band 5 (6^+) at 523.8 keV and the spins of the levels in band 4 were inferred from theoretical arguments (see discussion). The other spins in bands 5 and 6 were attributed relative to this 6^+

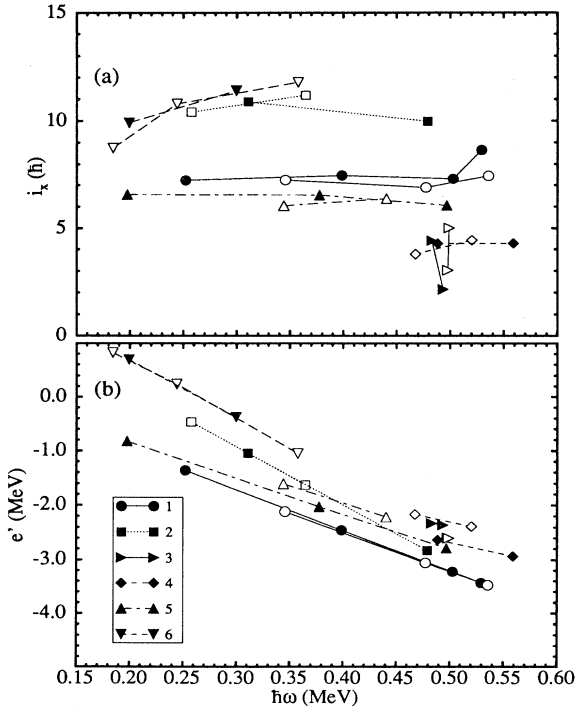

FIG. 3. Experimental quasiparticle (a) alignments and (b) Routhians for the six rotational bands of ^{108}Ag. The solid symbols correspond to α=0 and the open ones to α=1. The following symbols are used for the bands: circles band 1, squares band 2, diamonds band 4, triangles right, up and down bands 3, 5, and 6, respectively.

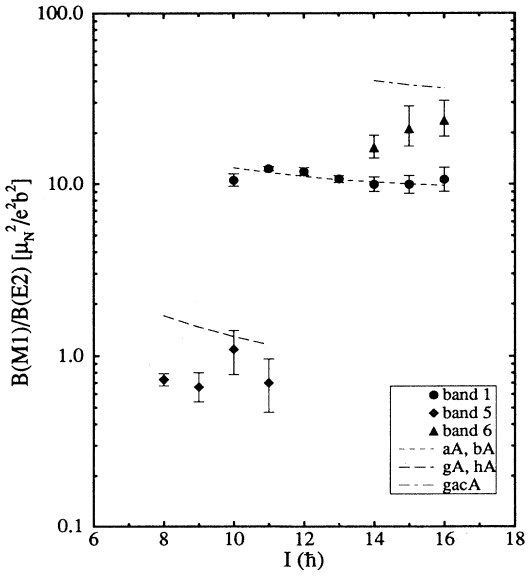

FIG. 4. Experimental and calculated $B(M1)/B(E2)$ ratios for bands 1, 5, and 6 in ^{108}Ag. The calculations were made using the deformation parameters $\beta_2 = 0.16$, $\beta_4 = 0$, $\gamma = 0°$ and $K = 4, 2$, and 8 for bands 1, 5, and 6, respectively. Circles band 1, diamonds band 5, and triangles up band 6.

bandhead and are consistent with the DCOQ results.

The experimental Routhians and alignments (Fig. 3) were calculated following the procedure described in [15,16] with the Harris parameters of $\mathcal{J}_0 = 3.6\ \hbar^2\text{MeV}^{-1}$ and $\mathcal{J}_1 = 29.8\ \hbar^4\text{MeV}^{-3}$, giving a nearly constant alignment for band 1. The K values used, experimental signature splittings, and proposed configurations are given in Table III.

The experimental in-band branching ratios $I_\gamma(\Delta I = 1)/I_\gamma(\Delta I = 2)$ from each level of spin I can provide valuable information regarding the intrinsic configuration of the band. The intensities I_γ were obtained from the spectra gated by the transitions populating the level of interest. Experimental reduced transition probability ratios can be obtained as

$$\frac{B(M1; I \to I-1)}{B(E2; I \to I-2)} = 0.693 \frac{1}{1+\delta^2} \frac{[E_\gamma(I \to I-2)]^5}{[E_\gamma(I \to I-1)]^3} \frac{I_\gamma(I \to I-1)}{I_\gamma(I \to I-2)}.$$

The results obtained for bands 1, 5, and 6 ($\delta = 0$) can be seen in Fig. 4, together with theoretical estimates (described in the Discussion). No reliable results were obtained for the other bands due to the poor statistics.

IV. THEORETICAL CALCULATIONS AND RESULTS

A. Quasiparticle Routhians

Figure 5 shows the quasiparticle Routhians calculated from the cranked shell model based on a deformed Woods-Saxon potential including monopole pairing interaction [17]. The diagrams are specific for $Z = 47$ and $N = 61$. The states are classified by the two remaining symmetries, parity and signature (π, α). The signature splitting for each configuration can be read off the diagrams. The aligned angular momentum (i_x) can be obtained from the derivative of the Routhian with respect to the rotational frequency: $i_x = -de'/d\omega$. Table IV shows the correspondence between the letter code used to specify the various quasiparticle states, parity, signature, Nilsson labels, and spherical shell model states most closely related.

It can be seen that the first band crossing occurs around $\hbar\omega = 0.35$ MeV and corresponds to the alignment of the first two $h_{11/2}$ quasineutrons (A and B) with the axis of rotation. The next crossing corresponds to the breaking of the first $g_{9/2}$ quasiproton pair (ab), around $\hbar\omega = 0.48$ MeV. The signature splitting between the a and b quasiprotons is small, which reflects the fact that the quasiprotons are weakly coupled to the rotational axis.

The deformation parameters used ($\beta_2 = 0.16$, $\beta_4 = 0$, $\gamma = 0°$) were chosen in accordance with the TRS calculations (see next section), and are appropriate, in general, to the bands which present at least one $\nu h_{11/2}$ quasineutron excitation.

TABLE IV. The letter code used to denote the quasiparticle states.

j shell	$[Nn_z\Lambda]\Omega$	Parity	$\alpha = -\frac{1}{2}$	$\alpha = +\frac{1}{2}$
$\nu h_{11/2}$	$[550]\frac{1}{2}$	-	A	B
$\nu h_{11/2}$	$[541]\frac{3}{2}$	-	C	D
$\nu g_{7/2}$	$[413]\frac{5}{2}$	+	E	F
$\nu d_{5/2}$	$[402]\frac{5}{2}$	+	G	H
$\pi g_{9/2}$	$[413]\frac{7}{2}$	+	b	a
$\pi g_{9/2}$	$[404]\frac{9}{2}$	+	d	c
$\pi g_{9/2}$	$[422]\frac{5}{2}$	+	f	e
$\pi(p_{1/2}, f_{5/2})$	$[301]\frac{1}{2}$	-	h	g

B. Equilibrium deformations

Standard total Routhian surface calculations were performed for the least excited configurations of ^{108}Ag. The calculations employ a deformed Woods-Saxon potential and a monopole pairing residual interaction [17,18]. The results are summarized in Fig. 6 which show the contour plots for the total energy in the intrinsic frame (mini-

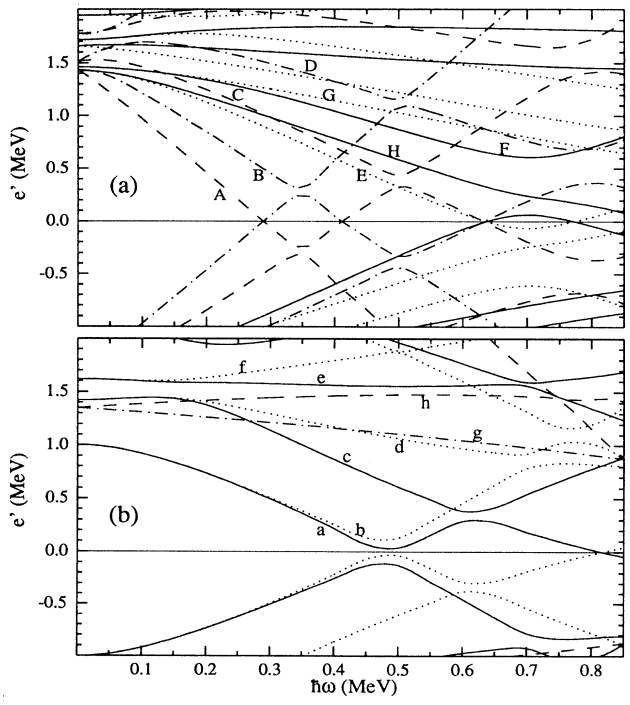

FIG. 5. Quasiparticle Routhians as a function of rotational frequency in ^{108}Ag for (a) neutrons and (b) protons ($\beta_2 = 0.16$, $\beta_4 = 0$, $\gamma = 0°$). The following convention is used for the levels: solid line ($\pi = +, \alpha = +\frac{1}{2}$), dotted line ($\pi = +, \alpha = -\frac{1}{2}$), dashed-dotted line ($\pi = -, \alpha = +\frac{1}{2}$), dashed line ($\pi = -, \alpha = -\frac{1}{2}$).

mized with respect to β_4) as a function of the deformation parameters β_2 and γ. The equilibrium deformation is indicated by the position of a thick dot.

Figures 6(a,b) show the results for the yrast configuration aA at two different rotational frequencies. The equilibrium is stable at a prolate-collective shape ($\gamma \approx 0°$) for a wide frequency range ($\hbar\omega = 0.2 - 0.5$ MeV) where the calculations were performed. The results are essentially the same for the theoretically unfavored signature $\alpha = 1$ (bA).

Figure 6(c) shows the result for the gA configuration (the positive parity configuration with the lowest excitation energy). The energy minimum is close to the one for the aA configuration but is very shallow with respect to γ. It fluctuates slightly around $\gamma = 0°$ as a function of frequency according to our calculations. The same is true for the unfavored signature configuration hA.

Figures 6(d,e,f) show the results for the aG configuration at three different frequencies. Below $\hbar\omega = 0.4$ MeV the energy minimum remains close to $\beta_2 = 0.1$, $\gamma = -120°$, representing a noncollective prolate state with about $6\hbar$ of angular momentum aligned with the symmetry axis. Above $\hbar\omega = 0.4$ MeV the configuration changes adiabatically into the $aABG$ configuration which contains the first aligned pair of $h_{11/2}$ quasineutrons (AB). As a consequence of the strong driving forces of the AB pair, the equilibrium deformation becomes prolate collective ($\beta_2 = 0.16$, $\gamma = 0°$). As a result of the collective rotation and the combined alignment of the four quasiparticles, the total spin for this configuration is at least $16\hbar$. A band based on this configuration is unlikely to be populated by the reaction used in this paper due to the limitation in the input angular momentum. This calculation is representative of other configurations containing one positive parity quasineutron and a $g_{9/2}$ quasiproton, viz., aE, aF, aH. This is rather surprising since the $g_{9/2}$ quasiproton has also a rather strong shape driving force. Oblate- or triaxial-collective deformations were previously expected for these positive parity configurations [7]. On the other hand it is possible to conclude from these calculations that the strong β_2 and γ driving properties of the $\nu h_{11/2}$ intruder orbit apparently tend to stabilize the equilibrium deformation around $\beta_2 = 0.16$, $\gamma = 0°$, rather independently of the other quasiparticles present.

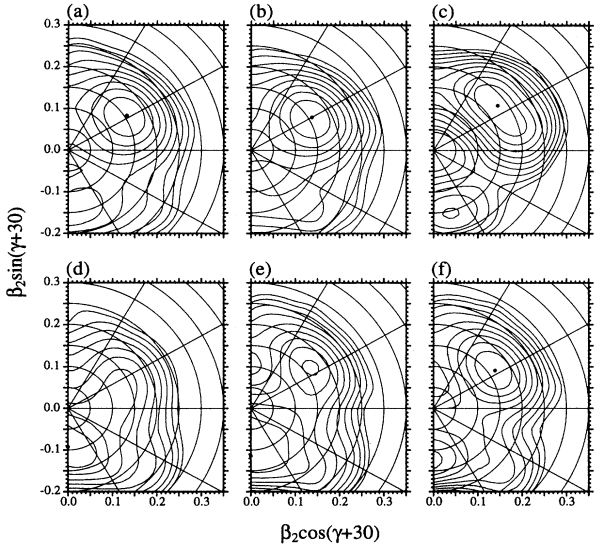

FIG. 6. Total Routhian surfaces for ^{108}Ag. (a) aA configuration, $\hbar\omega$=0.251 MeV (β_2=0.156, β_4=0.001, $\gamma = 2.2°$). (b) aA configuration, $\hbar\omega$=0.377 MeV (β_2=0.158, β_4=0.002, $\gamma = 0.0°$). (c) gA configuration, $\hbar\omega$=0.377 MeV (β_2=0.180, β_4=0.013, $\gamma = 6.5°$). (d) aG configuration, $\hbar\omega$=0.314 MeV (β_2=0.092, β_4=0.006, $\gamma = -120.0°$). (e) aG configuration, $\hbar\omega$=0.377 MeV (β_2=0.114, β_4=0.009, $\gamma = -120.0°$). (f) aG configuration, $\hbar\omega$=0.440 MeV (β_2=0.166, β_4=0.000, $\gamma = 3.2°$). The thick dots indicate the position of the equilibrium deformation.

C. Estimated branching ratios $B(M1)/B(E2)$

The theoretical branching ratios $B(M1)/B(E2)$ between in-band $\Delta I = 1$ and $\Delta I = 2$ transitions from each band state can be estimated from the geometrical model proposed by Dönau and Frauendorf [16]. In this semiclassical model the $M1$ transitions are assumed to originate from the precession of the magnetic moment vector around the total angular momentum vector. The intensity of the radiation is therefore proportional to the component of the magnetic moment vector perpendicular to the spin axis. Effective g factors are used to relate the angular momentum of each quasiparticle configuration to its magnetic moment vector. The estimates are then made from assumptions with respect to the orientation of the angular momentum of each quasiparticle, parametrized by the alignment and the projection onto the symmetry axis (K). The effective g factors are obtained from the Schmidt estimates, with an attenuation factor of 0.7 for the spin g-factors g_s [19].

The calculated branching ratios for the relevant configurations of ^{108}Ag can be compared to the experimental results in Fig. 4 (see also Sec. V). The deformation parameters used were $\beta_2 = 0.16$, $\beta_4 = 0$, $\gamma = 0°$, and the alignments of each quasiparticle were obtained from Fig. 5. For the aA and bA configurations, a $K = 4$ projection was assumed, arising essentially from the $g_{9/2}$ quasiproton (a, b). The $h_{11/2}$ quasineutron A is almost fully aligned ($i_x = 5.2\hbar$). In this situation the perpendicular components of the magnetic moments of the two quasiparticles tend to add, since the neutron g factor is negative and the proton positive, leading to rather high $M1$ transitions. The estimates shown for the gA, hA configurations are actually upper limits, calculated assuming the g factor of a pure $f_{5/2}$ ($g = 0.548$) component for the g, h quasiparticles and $K = 2$. For a fully rotation-aligned $\pi p_{1/2} \otimes \nu h_{11/2}$ configuration no $M1$ transitions are expected. The actual states g, h are of mixed $p_{1/2}, f_{5/2}$ parentage. For the $K = 8$ band ($gacA$), with a pair of $g_{9/2}$ quasiprotons (ac) coupled to the deformation

axis, very large $B(M1)/B(E2)$ ratios are calculated. A value of $K = 7$ would reduce the $B(M1)/B(E2)$ values by roughly 50%.

V. DISCUSSION

A. Bands 1 and 2

Band 1 is the yrast band and presents strong $M1$ transitions and weak $E2$ crossovers. The signature splitting is ≈ 60 keV at $\hbar\omega = 0.35$ MeV, decreasing as the frequency increases. This type of semidecoupled band is characteristic of a "conflicting" coupling between two intruder-orbit quasiparticles in odd-odd nuclei. We assign the $\pi g_{9/2} \otimes \nu h_{11/2}$ (aA and bA) configurations for this band, which corresponds to the lowest two quasiparticle excitations available. Bands with this configuration have been observed in other odd-odd Ag isotopes [2–4]. TRS calculations [see Fig. 6(a)] predict nearly axially symmetric prolate equilibrium deformations and a signature splitting of ≈ 35 keV (around $\hbar\omega = 0.35$ MeV), essentially the splitting between the a and b quasiproton orbits of opposite signatures [see Fig. 5(b)]. However, the theoretically favored signature is $\alpha = 0$ while experimentally it is $\alpha = -1$ (the same is true for the other odd-odd Ag and Rh isotopes cited in Sec. I). The quasiproton Routhians show signature inversion (with very small splitting) for γ between 10° and 20°. Indeed the TRS minima show a weak tendency toward positive γ values insufficient, though, to produce signature inversion.

For $\gamma \approx 0°$ the angular momenta of the two quasiparticles are nearly perpendicular to each other. This results, according to the geometrical model, in rather large $B(M1)/B(E2)$ ratios as shown in Fig. 4. The alignment expected for this configuration comes mostly from the quasineutron, which contributes with $5.2\hbar$, while the deformation aligned quasiproton contributes with about $2.7\hbar$, in reasonable agreement with the experimental result of $7.3\hbar$ [Fig. 3(a)]. The first neutron and proton crossings, AB and ab, respectively, are blocked for this configuration. The next two crossings expected are the BC (at $\hbar\omega = 0.51$ MeV) and the EF (around $\hbar\omega = 0.7$ MeV). We believe that the BC crossing is responsible for the upbend observed around $\hbar\omega = 0.53$ MeV [Fig. 3(a)]. Band 2 has negligible signature splitting and presents a gain in alignment of about $3.8\hbar$ relative to band 1. This is close to the expected alignment ($i_x = 4.2\hbar$) from the EF quasiparticles. On the other hand, the BC quasiparticles would contribute with an alignment of about $6.9\hbar$, therefore we tentatively assign the $aAEF$ and $bAEF$ configurations for band 2. The calculated splitting between the above configurations is ≈ 20 keV, around $\hbar\omega = 0.35$ MeV. The extrapolated crossing frequency between band 2 and band 1 lies above the upbend in band 1, which is qualitatively consistent with the present assignment. A band with similar characteristics to band 2 has been observed in ^{106}Ag by Popli *et al.* [2] and Jerrestam *et al.* [4]. The latter authors seem to suggest a $\pi g_{9/2} \otimes \nu(h_{11/2})^2(g_{7/2}, d_{5/2})$ configuration for this band. However, our calculations predict too large an alignment ($i_x = 6.8\ \hbar$) relative to band 1 for this configuration.

B. Bands 3 and 4

Both bands 3 and 4 present large signature splitting (250 keV and 350 keV, respectively), strong $E2$ transitions, and weak or absent $M1$ transitions. The 6^+ isomer has been interpreted as $[\pi(g_{9/2})^{-3} \otimes \nu d_{5/2}]_{6^+}$ coupled to the ^{110}Sn core [14]. This would correspond to the aG, $\alpha = 0$ configuration (and aH for the favored signature $\alpha = 1$). We believe that this state is the bandhead of band 3. A similar band has also been observed above the 6^+ isomer of ^{106}Ag. The equilibrium deformation for this configuration is calculated to be around $\beta_2 = 0.1$, $\gamma = -120°$, i.e., slightly prolate, noncollective (Fig. 6) for frequencies below 0.4 MeV which might be interpreted as the $I = 6$ bandhead. Above 0.4 MeV the miminum is shifted to $\beta_2 = 0.16$, $\gamma = 0°$ (prolate, collective) as a result of the alignment of the prolate-driving AB quasineutrons. For the latter deformation a small signature splitting, an alignment of $13\hbar$, and strong $M1$ transitions as in the case of band 1, are expected, in evident contradiction with the experiment. Experimentally, band 3 is observed at $\hbar\omega \approx 0.47$ MeV. TRS calculations show that, as the frequency approaches 0.4 MeV, the total energy minimum becomes shallow, extending toward oblate-collective deformations. Oblate or triaxial deformations could account for an increase in signature splitting between the $g_{9/2}$ quasiprotons and for the absence of strong $M1$ transitions. The AB crossing is also shifted to larger frequencies and therefore no contribution to the alignment is expected from the AB quasiparticles. However, no clear explanation is available for the steady increase in alignment of band 3, which might be an indication of either deformation changes or quasiparticle alignment. More detailed calculations as well as experimental results are necessary to resolve these difficulties.

Similar TRS results are obtained for the aH (the unfavored signature of band 3), bG, bH, aE, aF, bE, and bF configurations, since the natural parity (+) quasineutron orbits present a rather weak dependence on β_2 and γ. We tentatively assign the aE and aF (aE, bE would also be possible) configurations to the favored and unfavored signatures of band 4. The spin of the levels in band 4 were chosen to be consistent with this assignment.

C. Bands 5 and 6

Band 5 shows a rather constant alignment of 6–$6.5\hbar$ in the frequency range from 0.2 to 0.5 MeV and a large signature splitting (200 keV). The absence of the neutron AB crossing (predicted to be at $\hbar\omega \approx 0.35$ MeV) and the large alignment is a clear indication of the presence of a $h_{11/2}$ quasineutron (A) in the configuration of this band. The signature splitting of 200 keV is close

to those calculated for both the $(p_{1/2}, f_{5/2})$ (g,h) and the second $g_{9/2}$ (c,d) quasiproton excitations. The calculated signature splitting of the latter configuration is strongly dependent on frequency, while the experimental one is constant. In addition, at low spins the experimental $B(M1)/B(E2)$ ratios are rather small (around 0.6 $\mu_N{}^2/e^2b^2$). For a fully aligned (doubly decoupled) pure $\pi p_{1/2} \otimes \nu h_{11/2}$ configuration no $M1$ transitions are expected at all $[B(M1)/B(E2) = 0]$. However, admixtures from $p_{1/2}$, $f_{5/2}$, and $p_{3/2}$ are present in the first two negative parity quasiproton excitations (g,h), increasing the effective g factor and the quasiparticle angular momentum projection along the symmetry axis (K). Figure 4 shows the theoretical estimates for the limit of pure $\pi f_{5/2} \otimes \nu h_{11/2}$ $(K = 2)$ configuration (dashed line). On the other hand, the presence of the $g_{9/2}$ quasiproton would lead to $M1$ transitions an order of magnitude stronger. In view of the above arguments we propose gA, hA for the 1 and 0 signatures of band 5, respectively. Also in the odd isotopes (^{105}Ag, ^{107}Ag) [7,6], admixed $\pi p_{1/2}$ bands have been observed with similar characteristics. We estimate $I = 6\hbar$ for the bandhead assuming $I = I_x = i_{x\pi} + i_{x\nu} \approx 0.5 + 5.5 = 6\hbar$ for this rotation aligned band.

Band 6 decays to band 5 around $I = 12\hbar$. The experimental signature splitting is negligible and the experimental $B(M1)/B(E2)$ ratios surprisingly show an increase of more than an order of magnitude relative to band 5, which points toward a major configuration change. The above-mentioned characteristics of band 6 indicate a large K value. A $(\pi g_{9/2})^2$ configuration is known to produce $K^\pi = 8^+$ isomers in neighboring even-even Cd isotopes [20,21], and related high-K bands in odd Cd isotopes [22]. The possibility of the coupling of $[\pi g_{9/2}{}^2]_{K=8}$ to the configuration of band 6 was considered, and provides a possible explanation for the negligible signature splitting and in particular, the large $B(M1)/B(E2)$ ratios observed (this configuration is labeled $gacA$ in Fig. 4). However, it is puzzling that such a presumably large change in K value from band 6 to band 5 does not result in an observable delay in the interband transitions. The experimental setup of this paper is sensitive to lifetimes above 20 ns.

VI. CONCLUSION

A level scheme for the states populated in a heavy ion reaction has been proposed for ^{108}Ag. Six bandlike structures are observed. Tentative configuration assignments were proposed for each band by combining low-lying quasiproton excitations of $g_{9/2}$, $(p_{1/2}, f_{5/2})$ parentage, with quasineutron excitations of $h_{11/2}$, $g_{7/2}$, $d_{5/2}$. Similar structures have been observed by previous experiments in other nearby odd-odd or odd-A Ag isotopes. Most of the band structures observed can be understood within the cranked shell model. A weakly deformed prolate shape is predicted by TRS calculations for the configurations containing at least one $h_{11/2}$ quasineutron excitation. This prediction seems to be consistent with the data presently available. The band developed above the 6^+ isomer appears to have characteristics of triaxial or oblate shapes and cannot be fully understood with the present TRS calculations which predict only prolate axially symmetric shapes at moderate rotational frequencies. More detailed calculations with parameters optimized specifically for the ^{108}Ag region might clarify these matters.

ACKNOWLEDGMENTS

This work was partially supported by the Conselho Nacional de Desenvolvimento Científico e Tecnológico (CNPq), Coordenação de Aperfeiçoamento de Pessoal de Nível Superior (CAPES), and Fundação de Amparo à Pesquisa do Estado de São Paulo (FAPESP).

[1] T. Komatsubara, K. Furuno, T. Hosoda, J. Mukai, T. Hayakawa, T. Morikawa, Y. Iwata, N. Kato, J. Espino, J. Gascon, N. Gjørup, G.B. Hagemann, H.J. Jensen, D. Jerrestam, J. Nyberg, G. Sletten, B. Cederwall, and P.O. Tjøm, Nucl. Phys. **A557**, 419c (1993), and references therein.

[2] R. Popli, F.A. Rickey, L.E. Samuelson, and P.C. Simms, Phys. Rev. C **23**, 1085 (1981).

[3] J. Tréherne, J. Genevey, S. André, R. Béraud, A. Charvet, R. Duffait, A. Emsallem, M. Meyer, C. Bourgeois, P. Kilcher, J. Sauvage, F.A. Beck, and T. Byrski, Phys. Rev. C **27**, 166 (1983).

[4] D. Jerrestam, W. Klamra, J. Gizon, F. Lidén, L. Hildingsson, J. Kownacki, Th. Lindblad, and J. Nyberg, Nucl. Phys. **A577**, 786 (1994).

[5] R. Duffait, A. Charvet, K. Deneffe, R. Beraud, A. Emsallem, M. Meyer, T. Ollivier, J. Tréherne, A. Gizon, F. Beck, and T. Byrski, Nucl. Phys. **A454**, 143 (1986).

[6] R. Popli, J.A. Grau, S.I. Popik, L.E. Samuelson, F.A. Rickey, and P.C. Simms, Phys. Rev. C **20**, 1350 (1979).

[7] H.J. Keller, S. Frauendorf, U. Hagemann, L. Käubler, H. Prade, and F. Stary, Nucl. Phys. **A444**, 261 (1985).

[8] V.R. Vanin and M. Aïche, Nucl. Instrum. Methods Phys. Res. Sect. A **284**, 452 (1989).

[9] W.T. Milner, VAXPAK programs, Oak Ridge National Laboratory (1986).

[10] K.S. Krane, R.M. Steffen, and R.M. Wheeler, Nucl. Data Tables **11**, 351 (1973).

[11] J.E. Draper, Nucl. Instrum. Methods Phys. Res. Sect. A **247**, 481 (1986).

[12] G.K. Rochester and K.F. Smith, Phys. Lett. **8**, 266 (1964).

[13] O.C. Kistener and A.W. Sunyar, Phys. Rev. **143**, 918 (1966).

[14] T. Hattori, M. Adachi, and H. Taketani, J. Phys. Soc. Jpn. **41**, 1830 (1976).

[15] R. Bengtsson and S. Frauendorf, Nucl. Phys. **A237**, 139 (1979).

[16] F. Dönau and S. Frauendorf, in *Proceedings International Conference on High Spin Properties of Nuclei*, Oak Ridge, 1982, edited by N.R. Johnson (Harwood, New York, 1983) Nucl. Sci. Res. Ser., Vol **4**, p. 143.

[17] R. Wyss, J. Nyberg, A. Johnson, R. Bengtsson, and W. Nazarewicz, Phys. Lett. B **215**, 211 (1988).

[18] W. Nazarewicz, J. Dudek, R. Bengtsson, T. Bengtsson, and I. Ragnorsson, Nucl. Phys. **A435**, 397 (1985).

[19] S. Frauendorf, Phys. Lett. **100B**, 219 (1981).

[20] I. Thorslund, C. Fahlander, J. Nyberg, S. Juutinen, R. Julin, M. Piiparinen, R. Wyss, A. Lampinen, T. Lönnroth, D. Müller, S. Törmänen, and A. Virtanen, Nucl. Phys. **A564**, 285 (1993).

[21] S. Juutinen, R. Julin, M. Piiparinen, P. Ahonen, B. Cederwall, C. Fahlander, A. Lampinen, T. Lönnroth, A. Maj, S. Mitarai, D. Müller, J. Nyberg, P. Šimeček, M. Sugawara, I. Thorslund, S. Törmänen, A. Virtanen, and R. Wyss, Nucl. Phys. **A573**, 306 (1994).

[22] S. Juutinen, P. Šimeček, C. Fahlander, R. Julin, J. Kumpulainen, A. Lampinen, T. Lönnroth, A. Maj, S. Mitarai, D. Müller, J. Nyberg, M. Piiparinen, M. Sugawara, I. Thorslund, S. Törmänen, and A. Virtanen, Nucl. Phys. **A577**, 727 (1994).